Image Registration of DWI-T2w Images of the Prostate Gland

Afonso Raposo, *261379,* Adriana Hernando, *262891,* and Jurgena Gjuni, *265891*

***Abstract*—This assignment is concerned with the development of a semi-automatic system for the DWI-T2w alignment by selecting key points in the images. Rigid, affine and thin plate spline transformations are applied to MR images of the prostate gland.**

***Index Terms*—affine, DWI, image wrapping, MRI, rigid, T2W, thin plate spline**

I. Introduction

PROSTATE cancer is the second leading cause of cancer death in men in the United States [1]. T2-weighted (T2w) imaging combined with Diffusion weighted imaging (DWI) play an important role in the evaluation of patients with prostate cancer [2].

A. T2-weighted imaging

Using T2w imaging one can obtain morphological (anatomically correct) images of the prostate gland. Prostate cancer in this images normally shows a low signal intensity in contrast to the high intensity of the normal peripheral zone. MRI of prostate cancer with the conventional T2w imaging is predominantly limited to staging for the presence of extracapsular extension and seminal vesicle invasion, which might be too late for the patient.

B. Diffusion weighted imaging

Due to the recent hardware and software development, techniques like the DWI can be used for a better differentiation of cancer tissue from non-cancerous tissue.

This technique is a form of MRI based upon measuring the diffusion (motion) of water molecules within a voxel of tissue. Basically, we can expect tissues where water can diffuse very easily to appear darker, and tissues where water cannot move as easily (e.g., due to cell membranes getting in the way) to appear brighter. Images obtained using DWI are characterized as functional images, therefore they lack morphological information. This is where the DWI-T2w alignment comes to use.

C. DWI-T2w alignment

The purpose of this assignment is to develop a system to align the images obtained between these two forms of MR. To accomplish this goal, three different models of geometric transformation were implemented and analyzed: Rigid [3], Affine [4] and Thin-Plate Spline [5]. In order to evaluate the performance of each model, three metrics were used: Normalized Mutual Information [6], Normalized Cross-Correlation [7] and Target Registration Error.

II. Methods

In this section the three different geometric transformation will be explained as well as the three metrics used to evaluate the performance of the transformations.

A. Image Alignment

A geometric transformation transforms the set of coordinates (x, y) to (x', y'):

$$T(x, y) \rightarrow (x', y') \tag{1}$$

The objective of this transformation in this assignment was to fix the displacement of points in the DWI image compared to the T2w one.

Therefore, a set of points, treated as fixed points, were selected in the T2w image and a different set of corresponding points, moved points, were selected in the DWI image. The goal of applying a geometric transformation was to correspond each point of DWI to a point of T2w:

$$T(\text{fixed points}) \rightarrow \text{moved points} \tag{2}$$

$$T^{-1}(\text{moved points}) \rightarrow \text{fixed points} \tag{3}$$

If one can find the transformation T, can apply the same transformation to obtain the corresponding points between both images:

$$T(\mathrm{x_{T2w}}, \mathrm{y_{T2w}}) = (\mathrm{x_{DWI}}, \mathrm{y_{DWI}}) \tag{4}$$

$$T^{-1}(\mathrm{x_{DWI}}, \mathrm{y_{DWI}}) = (\mathrm{x_{T2w}}, \mathrm{y_{T2w}}) \tag{5}$$

1) Rigid transformation:

A rigid transformation is a geometric transformation that preserves the Euclidean distance between every pair of points.

The rigid transformation includes translation, rotation and reflection. In this assignment, since the images are not reflected horizontally or vertically, the reflection was not considered.

The transformation is characterized by the following expression:

$$\begin{bmatrix} x_m \\ y_m \\ 1 \end{bmatrix} = T_{\text{rigid}} \cdot \begin{bmatrix} x_f \\ y_f \\ 1 \end{bmatrix} \tag{6}$$

$$T_{\text{rigid}} = T_{\text{translation}} \cdot T_{\text{rotation}} \tag{7}$$

where (x_f, y_f) represent the coordinates of the "fixed" image and (x_m, y_m) the coordinates of the "moved" image,

T_{rigid} represents the rigid transformation matrix, $T_{\text{translation}}$ the translation matrix and T_{rotation} the rotation matrix.

A coordinates translation of $(x_{\text{trans}}, y_{\text{trans}})$ has the following translation matrix:

$$T_{\text{translation}} = \begin{bmatrix} 1 & 0 & x_{\text{trans}} \\ 0 & 1 & y_{\text{trans}} \\ 0 & 0 & 1 \end{bmatrix} \tag{8}$$

A coordinates rotation of θ has the following rotation matrix:

$$T_{\text{rotaion}} = \begin{bmatrix} \cos\theta & \sin\theta & 0 \\ -\sin\theta & \cos\theta & 0 \\ 0 & 0 & 1 \end{bmatrix} \tag{9}$$

The effect on the image will be something like this:

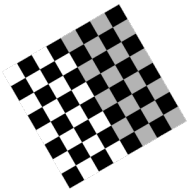

Fig. 1: Rotation transformation applied to a checkerboard image.

Since T_{rigid} is the multiplication of the previous two matrices, the rigid transformation matrix has the form:

$$T_{\text{rigid}} = T_{\text{translation}} \cdot T_{\text{rotation}} \tag{10}$$

$$T_{\text{rigid}} = \begin{bmatrix} 1 & 0 & x_{\text{trans}} \\ 0 & 1 & y_{\text{trans}} \\ 0 & 0 & 1 \end{bmatrix} \cdot \begin{bmatrix} \cos\theta & \sin\theta & 0 \\ -\sin\theta & \cos\theta & 0 \\ 0 & 0 & 1 \end{bmatrix} \tag{11}$$

$$T_{\text{rigid}} = \begin{bmatrix} \cos\theta & \sin\theta & x_{\text{trans}} \\ -\sin\theta & \cos\theta & y_{\text{trans}} \\ 0 & 0 & 1 \end{bmatrix} \tag{12}$$

Since the form of the rigid transformation is known, the relation between coordinates is:

$$\begin{bmatrix} x_m \\ y_m \\ 1 \end{bmatrix} = \begin{bmatrix} \cos\theta & \sin\theta & x_{\text{trans}} \\ -\sin\theta & \cos\theta & y_{\text{trans}} \\ 0 & 0 & 1 \end{bmatrix} \cdot \begin{bmatrix} x_f \\ y_f \\ 1 \end{bmatrix} \tag{13}$$

Which can be written as:

$$\begin{bmatrix} x_m \\ y_m \end{bmatrix} = \begin{bmatrix} \cos\theta & \sin\theta \\ -\sin\theta & \cos\theta \end{bmatrix} \cdot \begin{bmatrix} x_f \\ y_f \end{bmatrix} + \begin{bmatrix} x_{\text{trans}} \\ y_{\text{trans}} \end{bmatrix}$$

$$Q = R \cdot P + t \tag{14}$$

Where Q represents the moved points coordinates, R the rotation matrix, P the fixed points coordinates and t the translation matrix.

We then need to find a rigid transformation [8] that best aligns the two sets in the least squares sense, *i.e.*, we want a rotation R and a translation vector t such that:

$$(R, t) = \underset{R \in \mathbb{R}^{d\times d},\ t \in \mathbb{R}^d}{\operatorname{argmin}} \sum_{i=1}^{n} \left\| (R \cdot p_i + t) - q_i \right\|^2 \tag{15}$$

The challenge now is finding matrix R and vector t. To do so, let's assume R is fixed and denote:

$$F(t) = \sum_{i=1}^{n} \left\| (R \cdot p_i + t) - q_i \right\|^2 \tag{16}$$

We can find the optimal translation by taking the derivative of $F(t)$ and searching for it's *zeros*:

$$0 = \frac{\partial F(t)}{\partial t} = \sum_{i=1}^{n} 2(R \cdot p_i + t - q_i) =$$

$$= 2tn + 2R \cdot \sum_{i=1}^{n} 2p_i - 2 \cdot \sum_{i=1}^{n} q_i \tag{17}$$

By rearranging the Equation 17, we can get:

$$t = \bar{q} - R\bar{p} \tag{18}$$

In other words, the optimal translation t maps the transformed centroid of P, $\bar{p}$, to the centroid of Q, $\bar{q}$.

Plugging the optimal t in the Equation 16, we get:

$$F(t) = \sum_{i=1}^{n} \left\| (R \cdot p_i + t) - q_i \right\|^2 =$$

$$= \sum_{i=1}^{n} \left\| R \cdot p_i + \bar{q} - R\bar{p} - q_i \right\|^2 =$$

$$= \sum_{i=1}^{n} \left\| R \cdot (p_i - \bar{p}) - (q_i - \bar{q}) \right\|^2 \tag{19}$$

We can focus on computing the rotation R by restating the problem such that the translation would be zero:

$$x_i := p_i - \bar{p}, \quad y_i := q_i - \bar{q} \tag{20}$$

We're then searching for the optimal solution of R that:

$$R = \underset{R \in \mathbb{R}^{d\times d}}{\operatorname{argmin}} \sum_{i=1}^{n} \left\| R \cdot x_i - y_i \right\|^2 \tag{21}$$

We then computed the covariance matrix:

$$S = X^\top Y \tag{22}$$

where X and Y are the $d \times n$ matrices that have x_i and y_i as their columns, respectively.

If we apply the Singular Value Decomposition (SVD) [9] to the matrix S, we obtain:

$$S = U\Sigma V^\top \tag{23}$$

And, from [8], we know that the optimal values of R and t are:

$$R = V \begin{bmatrix} 1 & & & & \\ & 1 & & & \\ & & \ddots & & \\ & & & 1 & \\ & & & & \det(VU^\top) \end{bmatrix} U^\top \tag{24}$$

$$t = \bar{q} - R \cdot \bar{p} \tag{25}$$

2) AFFINE TRANSFORMATION*:*

The affine transformation [10] is a geometric transformation that preserves points, straight lines and planes. Similar to the rigid body transformation, the affine one has the form:

$$\begin{bmatrix} x_m \\ y_m \\ 1 \end{bmatrix} = T_{\text{affine}} \cdot \begin{bmatrix} x_f \\ y_f \\ 1 \end{bmatrix} \tag{26}$$

$$T_{\text{affine}} = T_{\text{translation}} \cdot T_{\text{rotation}} \cdot T_{\text{scale}} \cdot T_{\text{shear}} \tag{27}$$

The transformation matrices T_{scale} and T_{shear} are defined as follow:

$$T_{\text{scale}} = \begin{bmatrix} sc_x & 0 & 0 \\ 0 & sc_y & 0 \\ 0 & 0 & 1 \end{bmatrix}, \quad T_{\text{shear}} = \begin{bmatrix} 1 & 0 & sh_x \\ sh_y & 1 & 0 \\ 0 & 0 & 1 \end{bmatrix} \tag{28}$$

The transformation have the following result in images:

(a) Scale

(b) Shear

Fig. 2: Scale and shear transformations applied to a checkerboard image.

Fortunately, when considering the affine transformation matrix, one doesn't have to consider the contribution of each part individually, instead, can consider the affine transformation as whole. This means the affine transformation [11] form can be represent by a matrix with 6 unknown variables:

$$T_{\text{affine}} = \begin{bmatrix} T_{11} & T_{12} & T_{13} \\ T_{21} & T_{22} & T_{23} \\ 0 & 0 & 1 \end{bmatrix} \tag{29}$$

This makes possible the usage of the least squares [12] method to estimate the values of T_{affine} that best fit the fixed points to the moving points.

In simpler terms, the linear least squares (LS) method is used to discover the best approximation of the transformation that fits the data. Generally presented as in the Equation 30, the least squares method finds the vector x that fits A to b the best.

$$A \cdot x = b \tag{30}$$

To use the LS method, the Equation 26 needs to be reshaped to the shape of the Equation 30, so the least squares method can be applied:

$$\begin{bmatrix} x_f & y_f & 1 & 0 & 0 & 0 \\ 0 & 0 & 0 & x_f & y_f & 1 \end{bmatrix} \cdot \begin{bmatrix} T_{11} \\ T_{12} \\ T_{13} \\ T_{21} \\ T_{22} \\ T_{23} \end{bmatrix} = \begin{bmatrix} x_m \\ y_m \end{bmatrix} \tag{31}$$

After verifying that the Equations 26 and 31 are equivalents, one can write the matrix A (Equation 30) as:

$$A = \begin{bmatrix} x_{f1} & y_{f1} & 1 & 0 & 0 & 0 \\ 0 & 0 & 0 & x_{f1} & y_{f1} & 1 \\ x_{f2} & y_{f2} & 1 & 0 & 0 & 0 \\ 0 & 0 & 0 & x_{f2} & y_{f2} & 1 \\ \vdots & \vdots & \vdots & \vdots & \vdots & \vdots \\ x_{fn} & y_{fn} & 1 & 0 & 0 & 0 \\ 0 & 0 & 0 & x_{fn} & y_{fn} & 1 \end{bmatrix} \tag{32}$$

Where, x_{f1} represents the x coordinate of the first point of the n selected fixed points.

The affine transformation matrix corresponds to the unknown vector x, which has the form be:

$$x = \begin{bmatrix} T_{11} & T_{12} & T_{13} & T_{21} & T_{22} & T_{23} \end{bmatrix}^\top \tag{33}$$

and the vector b containing the moved points coordinates will be equal to:

$$b = \begin{bmatrix} x_{m1} & y_{m1} & x_{m2} & y_{m2} & \dots & x_{mn} & y_{mn} \end{bmatrix}^\top \tag{34}$$

The result of the ordinary least squares method, $\hat{x}$, is obtained by:

$$\hat{x} = (A^\top \cdot A)^{-1} \cdot A^\top \cdot b = A^\dagger \cdot b \tag{35}$$

In this case, to be able to apply the ordinary least squares method, one must provide, at least, three pairs of points (three fixed points and three moved points).

3) THIN-PLATE SPLINE TRANSFORMATION*:*

The thin-plate spline (TPS) is a data interpolation tool and the algebra behind it mimics the physical bending energy of a thin metal plate on point constraints.

The TPS has a closed-form solution, which allows the estimation of the parameters through the resolution of a linear system.

This transformation treats the deformed image as a 3-dimensional deformed plate of metal viewed from above, corresponding to a 2-dimensional plane. Hypothetically, this deformed sheet can be straightened out, obtaining the original plate of metal. If one applies the same concept to a 2-dimensional deformed image, the original (non deformed) image can be recovered.

Like before, both *fixed points* and *moved points* coordinates are known and are treated as *landmarks*.

The warping function for this transformation is defined as [13]:

$$f(x,y) = a_1 + a_2 x + a_3 y + \sum_{i=1}^{n} w_i U(\left|P_i - (x,y)\right|) \quad (36)$$

where (x, y) are coordinates on the warped ("fixed") image, $f(x, y)$ are coordinates on the deformed (moved) image, P_i are the selected landmarks on the deformed (moved) image with coordinates (x_{mi}, y_{mi}), n is the number of control points (landmarks); a_1, a_2, a_3 and w_i $(i = 1, \ldots, n)$ are the coefficients needed to be found. U is a radial basis function defined as:

$$-U(r) = r_{ij}^2 \log r_{ij}^2 \quad (37)$$

where r_{ij} is the Euclidean distance between points i and j. We can define the following matrices:

$$r_{ij} = \left|P_i - P_j\right| \quad , \quad P = \begin{bmatrix} 1 & x_{m1} & y_{m1} \\ 1 & x_{m2} & y_{m2} \\ \vdots & \vdots & \vdots \\ 1 & x_{mn} & y_{mn} \end{bmatrix} \quad (38)$$

The challenge here is to find the coefficients in Equation 36 that best fit the function f. Basically, the coefficients are obtained by "solving" the equation in order to, from the selected Fixed Points, obtain the selected Moved Points. This solutions is obtained as follow:

$$L^{-1}Y = (w_1 \; w_2 \ldots w_n \mid a_1 \; a_2 \; a_3) \quad (39)$$

where L and Y are defined as:

$$L = \begin{bmatrix} K & P \\ P^\top & 0 \end{bmatrix} \quad , \quad Y = (V \mid 0 \; 0 \; 0)^\top \quad (40)$$

The matrix P was defined previously. K and V are:

$$K = \begin{bmatrix} 0 & U(r_{12}) & \ldots & U(r_{1n}) \\ U(r_{21}) & 0 & \ldots & U(r_{2n}) \\ \vdots & \vdots & \ddots & \vdots \\ U(r_{n1}) & U(r_{n2}) & \ldots & 0 \end{bmatrix} \quad (41)$$

$$V = \begin{bmatrix} x_{f1} & x_{f2} & \ldots & x_{fn} \\ y_{f1} & y_{f2} & \ldots & y_{fn} \end{bmatrix} \quad (42)$$

Computing all the matrices described before, it's possible to obtain the TPS warping coefficients and apply the transformation to the deformed image.

What this do is map all the points of the warped image to corresponding points on the deformed image.

B. Metrics for Registration of Images

In order to evaluate the registration (alignment) performance, three metrics were adopted: Normalized Mutual Information, Normalized Cross-Correlation, since they are two of the most commonly used methods [14], and Target Registration Error.

1) Normalized Mutual Information:

Mutual information is an information theory measure of the statistical dependence between two random variables or the amount of information that one variable contains about the other [15].

It can be, in a general way, considered as a measure of how well one image explains the other. The most commonly used measure of information in image processing is the Shannon-Wiener entropy measure [7]:

$$\mathrm{H}(I) = -\sum_n p\{n\} \log(p\{n\}) \quad (43)$$

For an image, the entropy is calculated from the image intensity histogram in which the probabilities are the histogram entries:

$$p\{n\} = \frac{\text{\# pixels w/ color n}}{N} \quad (44)$$

where n represents the number of colors of the image, $n \in \{0, \ldots, 255\}$ in our case, and N represents the number of pixels of the image.

The joint entropy $H(\mathrm{I}_1, \mathrm{I}_2)$ can be calculated using the joint histogram of two images:

$$\mathrm{H}(\mathrm{I}_1, \mathrm{I}_2) = -\sum_{n_1} \sum_{n_2} p\{n_1, n_2\} \log(p\{n_1, n_2\}) \quad (45)$$

$$p\{n_1, n_2\} = \frac{\text{\# pixels w/ color } n_1 \text{ in } \mathrm{I}_1 \text{ and color } n_2 \text{ in } \mathrm{I}_2}{N} \quad (46)$$

Note: "# pixels w/ color n_1 in I_1 and color n_2 in I_2" increases by one every time $\mathrm{I}_1(x, y) = n_1$ and $\mathrm{I}_2(x, y) = n_2$.

Finally, the mutual information value is given by:

$$\mathrm{MI}(\mathrm{I}_1, \mathrm{I}_2) = \mathrm{H}(\mathrm{I}_1) + \mathrm{H}(\mathrm{I}_2) - \mathrm{H}(\mathrm{I}_1, \mathrm{I}_2) \quad (47)$$

After calculating the mutual information value between the two images, one can obtain the Normalized Mutual Information by [16]:

$$\mathrm{NMI}(\mathrm{I}_1, \mathrm{I}_2) = \frac{\mathrm{MI}(\mathrm{I}_1, \mathrm{I}_2)}{\sqrt{\mathrm{H}(\mathrm{I}_1) H(\mathrm{I}_2)}} \quad (48)$$

This will return a value between 0 and 1, where the value 1 means that the images are equal.

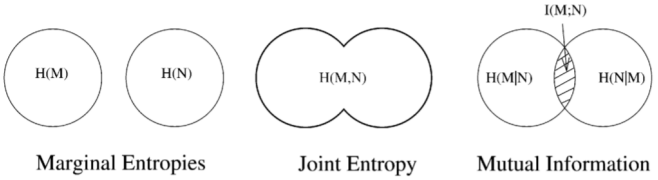

Fig. 3: A set theory representation of the entropies involved when combining two images. [6]

2) Normalized Cross-Correlation:

In signal processing, cross-correlation is used to measure how similar two signals are.

In image processing, cross-correlations is a standard approach for feature detection. It can be used as a measure for calculating the degree of similarity between two images [7].

To eliminate possible variations due to lighting and exposure conditions, the images can be first normalized. This is typically done by subtracting the mean and dividing by the standard deviation at every step [17].

Then, the function applied to each pixel of the image is:

$$\mathrm{I}_{\mathrm{NCC}}(x,y) = \frac{(\mathrm{I}_1(x,y)-\mu_1)(\mathrm{I}_2(x,y)-\mu_2)}{N\sigma_1\sigma_2} \tag{49}$$

where μ, σ and N represent the mean value, the standard deviation value and the number of pixels of one image, respectively.

This will result in a new image where the higher values represent regions of similarity and the lower values represent regions of dissimilarity.

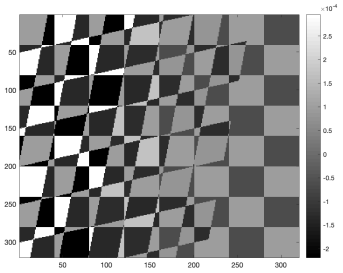

Fig. 4: Image obtained by applying the NCC equation to two misaligned checkerboard images.

All the values of the obtained image can be summed up to one number that will work as a method to comparatively evaluate similarity between two pairs of images, i.e., which pair of images is more similar to each other:

$$\mathrm{NCC}(\mathrm{I}_1,\mathrm{I}_2) = \sum_{x,y} \mathrm{I}_{\mathrm{NCC}}(x,y) \tag{50}$$

Since $NCC(\mathrm{I}_1,\mathrm{I}_1) = 1$ isn't necessarily true, the NCC expression was slightly altered to make sure that the NCC between two images equals 1 when the images are the same:

$$\mathrm{NCC}'(\mathrm{I}_1,\mathrm{I}_2) = \frac{\mathrm{NCC}(\mathrm{I}_1,\mathrm{I}_2)}{\mathrm{NCC}(\mathrm{I}_1,\mathrm{I}_1)} \tag{51}$$

Volume of Interest:

These two previous methods can be applied to images of the same typology, *e.g.*, one can use these two compare two R-ray images. But, when it's given the task to evaluate two images from different modalities, like T2w and DWI, even tho both are MRI images, since the same structure can appear with different values in each image, it's helpful to select the Volume of Interest in order to reduce the background bias.

The VOI corresponds to the rectangle whose center is the centroid of the Fixed Points, its width and height are equal to two times 150% of the maximum distance between x coordinates and y coordinates, respectively.

Examples are illustrated on Figure 5.

(Note: even tho the anus canal has no interest for this study, it was selected since its shape is easily recognizable and it might make easier to check the performance of the image alignment)

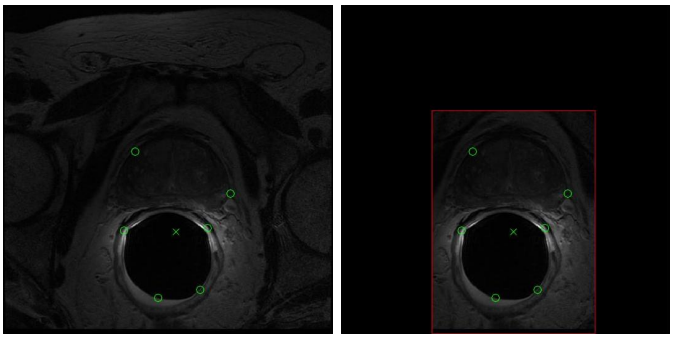

(a) T2 image (b) VOI of T2 image

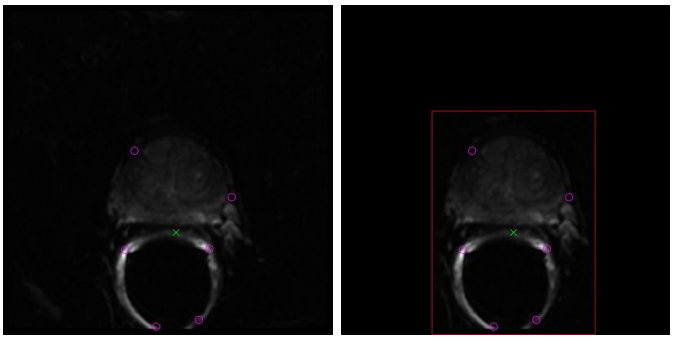

(c) DWI image (d) VOI of DWI image

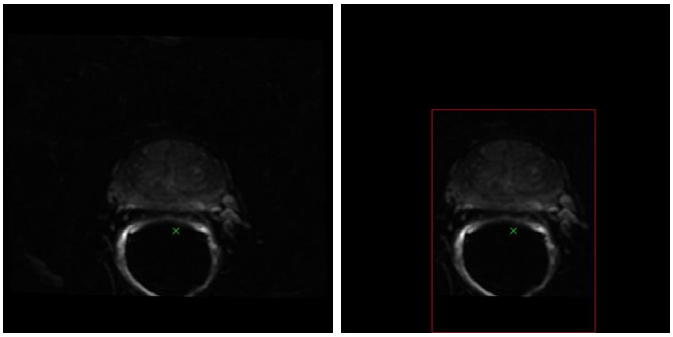

(e) DWI image after registration (f) VOI of DWI image (affine)

Fig. 5: Illustration of the VOI selection, where the green circles represent the Fixed Points, the magenta circles represent the Moved Points, the green cross represents the mentioned centroid and the red rectangle delimits the VOI area.

3) Target Registration Error:

This metric compares the distance between partner points before and after registration. In an ideal case, one wants the distance between partner points after registration to be equal to 0. The Euclidean distance was adopted to measure the distance between partner points.

$$d_b(i) = \left|(x_{fi}, y_{fi}) - (x_{mi}, y_{mi})\right| \tag{52}$$

After obtaining d_b and d_a which represent the distance between partner points before and after the transformation, respectively, we calculate the TRE as follow:

$$\delta_{TR} = 1 - \frac{1}{n}\sum_{i=1}^{n}\frac{d_b(i) - d_a(i)}{d_b(i)} \tag{53}$$

If the distance between partner points after the registration is equal to 0, which means the points are on the same position, the TRE will be equal to 0. If the distance between partner points didn't alter during the transformation the TRE will be 1. If the TRE is ≥ 1, the average distance between points increased during the registration.

III. Results

In this section we'll go over the results of the DWI-T2w registration, illustrating examples of each transformation and measuring the registration of each transformation (Rigid, Affine and Thin-Plate Splines) to one slice of each patient.

First, we present the three transformations applied to a checkerboard image, so one can verify the behaviour of each (Figure 6).

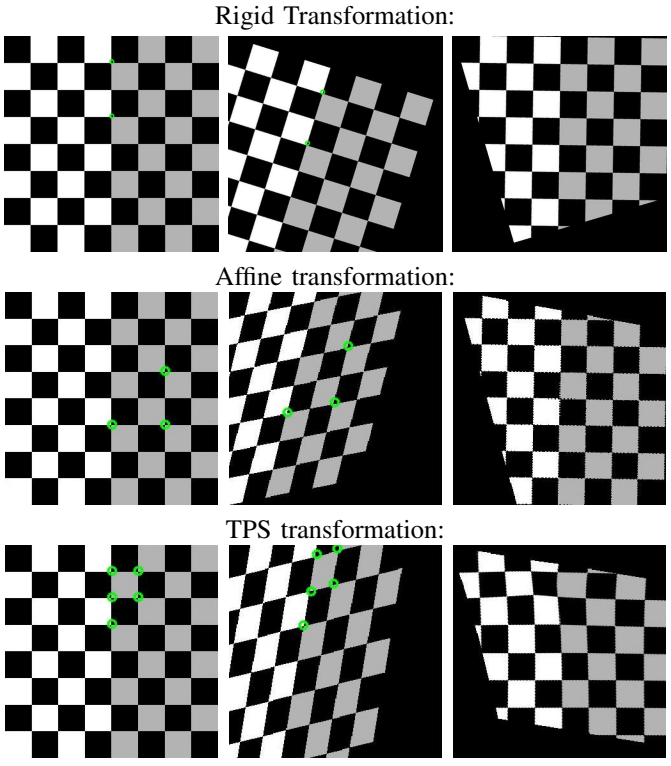

(a) Fixed (b) Moved (c) Warped

Fig. 6: Three image alignment methods applied to checkerboard images with different deformations. The green circles represent the points selected in each image.

We can observe that, generally, the three algorithms worked as supposed to. The evaluation of the registration for the previous examples is presented in the Table I.

TABLE I: Evaluation of the alignment of the checkerboard images.

		Rigid		**Affine**		**TPS**	
		before	after	before	after	before	after
Total image	NMI	0.0650	0.4283	0.0650	0.5267	0.0646	0.3596
	NCC	0.0252	0.4110	0.0256	0.3857	0.0211	0.3073
VOI	NMI	0.1580	0.8548	0.0408	0.7544	0.2889	0.6904
	NCC	0.3168	0.9642	0.1659	0.8912	0.5426	0.8235
TRE		0.0118		≈ 0		0.0037	

The next step was the registration of one slice of each volume/patient and the evaluation of this process.

This resulted in 25 images (Figure 7) from 25 different patients, all corresponding to the 12^{th} slice.

Then, 6 pairs of corresponding points were selected in each pair of T2w and DWI images and the 3 alignment methods (rigid, affine and TPS) were applied (Figure 7).

Applying the evaluation metrics (NMI, NCC and TRE) to the VOI of every image gathered, we obtained the results present in the Tables II, III and IV.

TABLE II: Results of the Target Registration error for each registration method.

		TRE		
Image	**Slice**	**Rigid**	**Affine**	**TPS**
IM0002	12	3.4791	0.4102	0.0757
IM0013	12	0.8691	0.1892	0.0270
IM0016	12	5.3973	2.6800	0.1395
IM0022	12	0.8803	0.8071	0.0275
IM0025	12	1.9888	0.5097	0.0444
IM0044	12	1.3700	0.2003	0.0305
IM2001	12	0.8222	0.4533	0.0247
IM2002	12	1.8800	0.6013	0.0406
IM2004	12	1.0895	0.2802	0.0187
IM2010	12	1.7462	0.1619	0.0438
IM2022	12	1.1142	0.5543	0.0320
IM3005	12	1.1288	0.5224	0.0373
IM3007	12	3.8645	0.5283	0.0856
IM3009	12	0.8600	0.5710	0.0688
IM3013	12	0.8204	0.1525	0.0337
IM3032	12	0.8620	0.3177	0.0279
IM3033	12	0.6025	0.3319	0.0146
IM3036	12	0.5714	0.3643	0.0393
IM3059	12	1.8549	1.2544	0.0539
IM3068	12	1.6344	1.2091	0.0807
IM3113	12	1.2575	0.3077	0.0471
IM3154	12	0.8469	0.5478	0.0707
IM3160	12	0.9403	0.9213	0.0888
IM3211	12	1.8030	1.9258	0.2917
IM3268	12	1.3060	0.7011	0.1167
Mean		1.5596	0.6601	0.0624

The discussion of these results will be one of the subjects of the next section.

IV. Discussion

There's a lot to say regarding the previous results.

First, let's discuss the results obtained in the Figure 6 and in the Table I.

Analyzing these, one can confirm that the registration algorithms are well built and are delivering the expected results.

Looking to the evaluation results, we can see that the Target Registration Error to each method is very low, indicating that

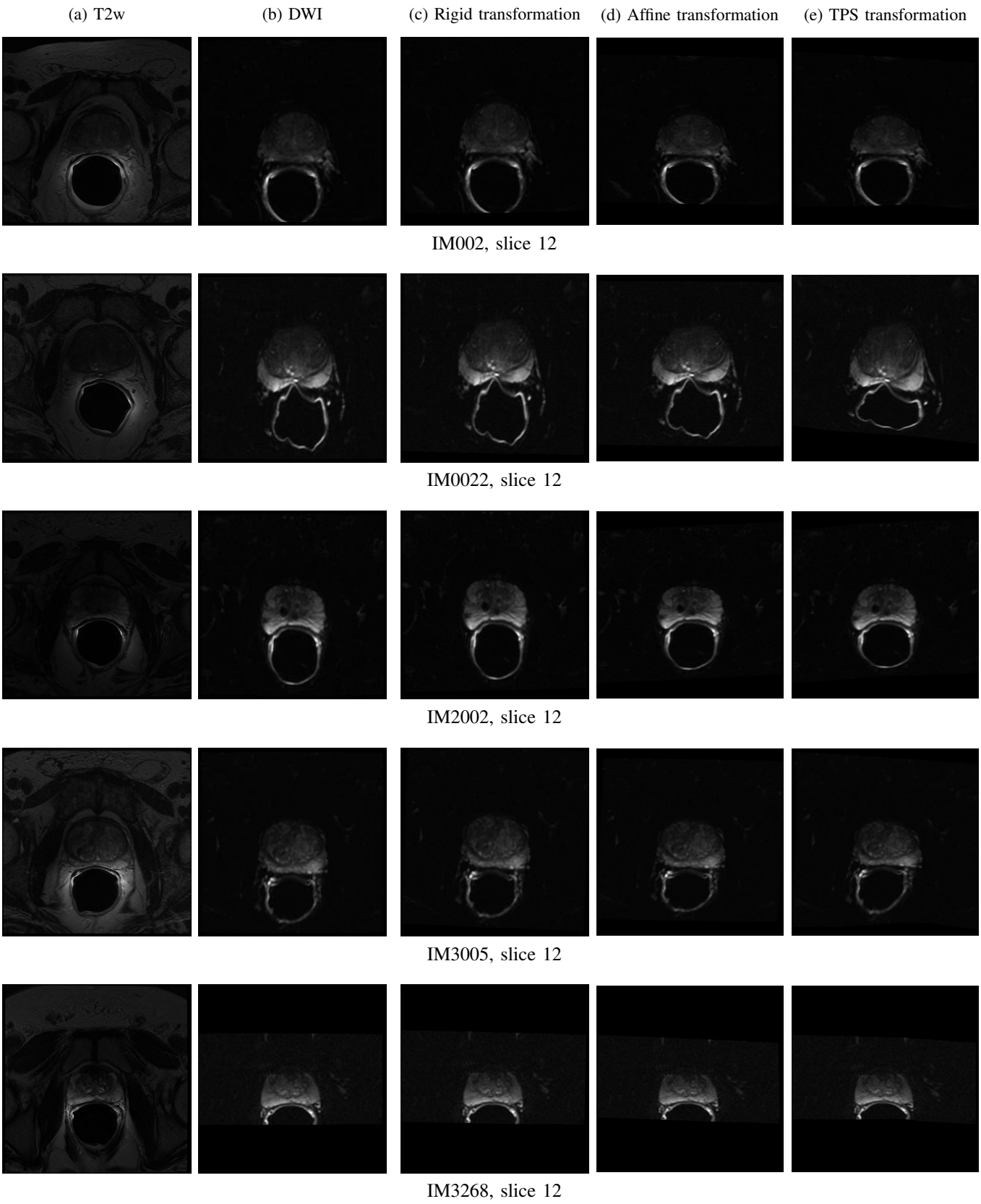

Fig. 7: Rigid, Affine and TPS registration used to align 5 images of DWI to their corresponding T2w image of the prostate gland. In each registration, 6 points were selected and the same group of points was used in each different registration method.

TABLE III: Results of the Normalized Mutual Information between T2w and DWI images. δ represents the variation of the NMI between the T2w-DWI images and T2w-warped images.

		NMI						
Image	**Slice**	**DWI**	**Rigid**	**Affine**	**TPS**	**δ Rigid (%)**	**δ Affine (%)**	**δ TPS (%)**
IM0002	12	0.3823	0.3553	0.3325	0.3413	-7.08	-13.05	-10.73
IM0013	12	0.3543	0.3310	0.3089	0.3366	-6.58	-12.83	-5.01
IM0016	12	0.3450	0.3216	0.2992	0.2996	-6.77	-13.26	-13.15
IM0022	12	0.2885	0.2601	0.2482	0.2302	-9.82	-13.96	-20.21
IM0025	12	0.3905	0.3831	0.3518	0.3572	-1.91	-9.91	-8.54
IM0044	12	0.4007	0.3634	0.3542	0.3575	-9.31	-11.60	-10.77
IM2001	12	0.4002	0.3789	0.3664	0.3797	-5.31	-8.44	-5.12
IM2002	12	0.3963	0.3955	0.3656	0.3573	-0.21	-7.76	-9.85
IM2004	12	0.3692	0.3310	0.3040	0.3307	-10.36	-17.67	-10.43
IM2010	12	0.4137	0.3855	0.3706	0.3860	-6.81	-10.43	-6.69
IM2022	12	0.4270	0.3740	0.3545	0.3448	-12.40	-16.98	-19.24
IM3005	12	0.3738	0.3452	0.3252	0.3366	-7.66	-12.99	-9.96
IM3007	12	0.4057	0.4008	0.3908	0.3866	-1.22	-3.69	-4.72
IM3009	12	0.4316	0.4266	0.4241	0.4261	-1.17	-1.76	-1.29
IM3013	12	0.3954	0.3579	0.3387	0.3333	-9.50	-14.35	-15.71
IM3032	12	0.3938	0.3846	0.3555	0.3630	-2.34	-9.72	-7.82
IM3033	12	0.4146	0.3639	0.3534	0.3526	-12.22	-14.78	-14.96
IM3036	12	0.4415	0.4298	0.4335	0.4334	-2.66	-1.81	-1.84
IM3059	12	0.3862	0.3789	0.3787	0.3891	-1.88	-1.93	0.77
IM3068	12	0.4350	0.4232	0.4162	0.4316	-2.71	-4.32	-0.79
IM3113	12	0.4134	0.4145	0.3957	0.3910	0.29	-4.26	-5.40
IM3154	12	0.3892	0.3815	0.3784	0.3837	-1.97	-2.76	-1.42
IM3160	12	0.2817	0.2703	0.2698	0.2734	-4.05	-4.20	-2.93
IM3211	12	0.4354	0.4279	0.4205	0.4264	-1.72	-3.42	-2.07
IM3268	12	0.3958	0.3958	0.3868	0.3847	0.01	-2.28	-2.79
Mean		0.3904	0.3712	0.3569	0.3613	-5.02	-8.73	-7.63

TABLE IV: Results of the Normalized Cross Correlation between T2w and DWI images. δ represents the variation of the NCC between the T2w-DWI images and T2w-warped images.

		NCC						
Image	**Slice**	**DWI**	**Rigid**	**Affine**	**TPS**	**δ Rigid (%)**	**δ Affine (%)**	**δ TPS (%)**
IM0002	12	0.3876	0.4581	0.4283	0.4714	18.19	10.50	21.62
IM0013	12	0.3291	0.3411	0.4145	0.4582	3.64	25.92	39.20
IM0016	12	0.4681	0.4988	0.4895	0.4849	6.55	4.57	3.60
IM0022	12	0.3455	0.3152	0.3264	0.3553	-8.76	-5.52	2.85
IM0025	12	0.3593	0.3865	0.3995	0.4085	7.56	11.20	13.69
IM0044	12	0.4852	0.4914	0.5275	0.5317	1.28	8.70	9.57
IM2001	12	0.4720	0.4159	0.4050	0.3971	-11.88	-14.19	-15.88
IM2002	12	0.4764	0.5218	0.5415	0.5134	9.54	13.66	7.77
IM2004	12	0.3562	0.3364	0.3383	0.3857	-5.57	-5.02	8.27
IM2010	12	0.4812	0.4726	0.4802	0.4982	-1.77	-0.19	3.54
IM2022	12	0.5719	0.5079	0.5321	0.5913	-11.19	-6.95	3.40
IM3005	12	0.5172	0.4854	0.4612	0.4541	-6.15	-10.84	-12.20
IM3007	12	0.5221	0.5490	0.5441	0.5684	5.15	4.22	8.88
IM3009	12	0.5648	0.4944	0.5280	0.5781	-12.48	-6.51	2.35
IM3013	12	0.5392	0.5397	0.5089	0.5232	0.08	-5.62	-2.97
IM3032	12	0.5583	0.5651	0.5410	0.5733	1.21	-3.09	2.68
IM3033	12	0.4818	0.4942	0.4827	0.5018	2.58	0.18	4.16
IM3036	12	0.6303	0.6830	0.6886	0.6770	8.36	9.25	7.41
IM3059	12	0.5713	0.5521	0.5678	0.5781	-3.37	-0.62	1.19
IM3068	12	0.7360	0.7403	0.7133	0.7247	0.59	-3.08	-1.53
IM3113	12	0.5456	0.6109	0.5905	0.6145	11.97	8.23	12.63
IM3154	12	0.7131	0.6626	0.6708	0.6694	-7.08	-5.93	-6.12
IM3160	12	0.5110	0.4771	0.4875	0.4818	-6.64	-4.61	-5.72
IM3211	12	0.6505	0.6849	0.6832	0.6880	5.29	5.03	5.77
IM3268	12	0.6971	0.7453	0.7620	0.7685	6.92	9.32	10.24
Mean		0.5188	0.5212	0.5245	0.5399	0.56	1.54	4.98

the initial position of each point was successfully approximated to its initial one.

If we look to the Normalized Mutual Information and Normalized Cross Correlation results, we can confirm that there was an improvement with each transformation. We can also see that these values show a higher value when considering only the VOI area, this is due to the fact that, generally, the registration algorithms focus on aligning the selected points, but this alignment might not occur as well on regions of the image farther from the selected points.

It's important mentioning that in the Rigid Transformation example, the "Moved" image was obtained by applying a Rigid Transformation, therefore, the successful recovery of the original image, which would not occur if the distance between points in the "Fixed" image and the "Moved" image was not maintained. Focusing on the Thin-Plate Spline transformation we can see that straight lines on the original image get deformed on the registration process.

Now analyzing the results regarding the registration methods applied to the prostate gland MR images, Figure 7 and Tables II, III and IV. First, one can verify the main advantage of using DWI images, the prostate gland is easily visible and some features of it become visible in this imaging method. Features that can help the diagnosis.

Unlike the previous example, looking at the image results, it's not simple to verify if the original image was recovered or not. Therefore, it's important to analyze the results obtained in the registration's evaluation. Starting with the TRE, Table II, we can verify that the TPS registration was the one who presented the lowest value, but it's important to remember that this registration can warp the image, losing straight lines, in order to approximate the "Moved" points to the "Fixed" points. This means that, even tho the TRE is the lowest, doesn't necessarily mean that the obtained image after this registration method is the most similar to the original ("Fixed") image.

The results of the NMI evaluation weren't like expected. We can see that it indicates that each Registration Method moved the image away from the original image, which is the opposite from the desired. However, the NCC results indicate the opposite. They indicate that the images obtained are more similar to the original ones. From our understanding, this is due to the fact that the same structures can appear with different values in the T2w and DWI images, and, since this methods evaluate the similarity of images regarding the location of the values and not the overall shapes in the image, these differences in the results arise. The NMI method analyses the probability of finding the same values in the same regions in both images, therefore, the values don't reflect the correct alignment of shapes in the image. On the other hand, the NCC also compares values in the same position, but this method compares the similarity of values, resulting in more accurate results. Because of this, we'll only consider the NCC values to evaluate the registration of the MRI images. Unfortunately, due to this limitations originated by the differences between the two MRI methods, we can only compare the three methods qualitatively.

We can see that, between the three registration methods, the TPS was the one which, overall, presented a bigger improvement of similarity between the T2w image and the aligned DWI image, indicating that this method is the best, between the three, to perform the registration. However, it's worth mentioning that the Affine transformation is the easiest to perform, since the calculations involved, Least Squares method, are simpler to do. Taking into account that the results presented are also positive, this method might be preferable to the others.

It's important to remember that these results come from only 25 samples, which might not be a sample size statistically relevant, and are dependent of the points selection in each image, which can widely alter the results obtained.

Nevertheless, the three registrations methods, Rigid, Affine and Thin-Plate Spline, were able to align the DWI images to the T2w images. The last one presented the best results.

For a future study, one could try to implement an automatic points selection algorithm in order to make the process unbiased and, regarding the evaluation algorithms, maybe apply a segmentation method to identify the prostate gland's shape in each image and then compare the different masks instead of the MRI images themselves.

REFERENCES

[1] Cancer.net, "Prostate cancer: Statistics," https://www.cancer.net/cancer-types/prostate-cancer/statistics, accessed January 12, 2019.

[2] N. M. AbdelMaboud, H. H. Elsaid, and E. A. Aboubeih, "The role of diffusion weighted mri in evaluation of prostate cancer," *The Egyptian Journal of Radiology and Nuclear Medicine*, vol. 45, 2014. [Online]. Available: https://www.sciencedirect.com/science/article/pii/S0378603X13001502

[3] Wikipedia, "Rigid transformation," https://en.wikipedia.org/wiki/Rigid_transformation, accessed January 12, 2019.

[4] ——, "Affine transformation," https://en.wikipedia.org/wiki/Affine_transformation, accessed January 12, 2019.

[5] F. L. Bookstein, "Principal warps: Thin-plate splines and the decomposition of deformations," *IEEE: Transactions on pattern analysis and machine intelligence*, vol. 11, no. 6, 1989.

[6] C. Studholme, D. Hill, and D. Hawkes, "An overlap invariant entropy measure of 3d medical image alignment," *Pattern Recognition*, vol. 32, 1999.

[7] V. Roshni and D. K. Revathy, "Using mutual information and cross correlation as metrics for registration of images," *Journal of Theoretical and Applied Information Technology*, vol. 2017, 2005.

[8] O. Sorkine-Hornung and M. Rabinovich, "Least-squares rigid motion using svd," 2017.

[9] Wikipedia, "Singular value decomposition," https://en.wikipedia.org/wiki/Singular_value_decomposition, accessed January 26, 2019.

[10] R. Hartley and A. Zisserman, *Multiple View Geometry in computer vision*, 2nd ed. Cambridge University Press, 2004.

[11] H. Spth, "Fitting affine and orthogonal transformations between two sets of points," *Mathematical Communications*, vol. 9, 2004.

[12] Wikipedia, "Linear least squares," https://en.wikipedia.org/wiki/Linear_least_squares, accessed January 12, 2019.

[13] Y. Liu, M. Uberti, H. Dou, R. L. Mosley, H. E. Gendelman, and M. D. Boska, "An image warping technique for rodent brain mri-histology registration based on thin-plate splines with landmark optimization," *Proceedings of SPIE - The International Society for Optical Engineering*, vol. 7259, 2009.

[14] L. Hao, Y. Huang, Y. Gao, X. Chen, and P. Wang, "Nonrigid registration of prostate diffusion-weighted mri," *Journal of Healthcare Engineering*, vol. 2017, 2017.

[15] Wikipedia, "Mutual information," https://en.wikipedia.org/wiki/Mutual_information, accessed January 23, 2019.

[16] A. Strehl and J. Ghosh, "Cluster ensembles a knowledge reuse framework for combining multiple partitions," *Journal of Machine Learning Research 3*, 2002.

[17] Wikipedia, "Cross-correlation," https://en.wikipedia.org/wiki/Cross-correlation, accessed January 23, 2019.